



Evaporation-induced self-assembled silica colloidal particle-assisted nanoporous structural evolution of poly(ethylene terephthalate) nonwoven composite separators for high-safety/high-rate lithium-ion batteries

Jung-Ran Lee^a, Ji-Hye Won^a, Jong Hun Kim^b, Ki Jae Kim^c, Sang-Young Lee^{a,*}

^a Department of Chemical Engineering, Kangwon National University, Chuncheon, Kangwondo 200-701, Republic of Korea

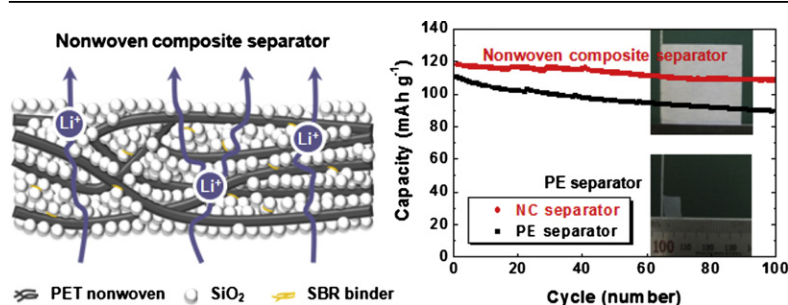
^b Batteries R&D, LG Chem, Yuseong-gu, Daejeon 305-380, Republic of Korea

^c Advanced Batteries Research Center, Korea Electronics Technology Institute, Seongnam, Gyeonggido 163-816, Republic of Korea

HIGHLIGHTS

- New nonwoven composite separators for use in high-safety/high-rate lithium batteries.
- Provision of a facile route to fine-tune porous structure of the nonwoven separators.
- Silica colloidal particle-assisted nanoporous structural evolution in PET nonwovens.
- Interstitial voids formed from evaporation-induced self-assembly of SiO₂ colloidal particles.
- The structural novelty allows lower thermal shrinkage and superior cell performance.

GRAPHICAL ABSTRACT



ARTICLE INFO

Article history:

Received 4 February 2012

Received in revised form

28 April 2012

Accepted 21 May 2012

Available online 27 May 2012

Keywords:

Lithium-ion batteries

High-safety/high-rate

Nonwoven composite separators

Colloidal silica particles

Evaporation-induced self-assembly

Nanoporous structure

ABSTRACT

A facile approach to the fabrication of nanoporous structure-tuned nonwoven composite separators is demonstrated for application in high-safety/high-rate lithium-ion batteries. This strategy is based on the construction of silica (SiO₂) colloidal particle-assisted nanoporous structure in a poly(ethylene terephthalate) (PET) nonwoven substrate. The nanoparticle arrangement arising from evaporation-induced self-assembly of SiO₂ colloidal particles allows the evolution of the unusual nanoporous structure, i.e. well-connected interstitial voids formed between close-packed SiO₂ particles adhered by styrene-butadiene rubber (SBR) binders. Meanwhile, the PET nonwoven serves as a mechanical support that contributes to suppressing thermal shrinkage of the nonwoven composite separator. The aforementioned structural novelty of the nonwoven composite separator plays a key role in providing the separator with advantageous characteristics (specifically, good electrolyte wettability, high ionic conductivity, and benign compatibility with electrodes), which leads to the better cell performance than a commercialized polyethylene (PE) separator.

© 2012 Elsevier B.V. All rights reserved.

1. Introduction

With rapid expansion of lithium-ion batteries into newly emerging application fields such as smart mobile devices, power tools, (hybrid, plug-in, and zero-emission) electric vehicles, and

* Corresponding author. Tel.: +82 33 250 6338; fax: +82 33 251 3658.
E-mail address: syleek@kangwon.ac.kr (S.-Y. Lee).

energy storage systems, which generally require high-energy density and high-power density, formidable challenges related to safety failures must be confronted [1–4]. In particular, in addressing internal short-circuit problems, which are believed to be the most critical threat in securing battery safety, a separator is considered a key component to suppress the failure, as its primary role is to maintain electrical isolation between the cathode and anode [5–7]. Another important function of separators is to allow ionic transport via their liquid electrolyte-filled micropores. The ionic conductivity of separators is known to heavily affect ohmic polarization (i.e., IR drop) of cells.

While currently widely used polyolefin-based separators have many advantages for use in lithium-ion batteries, their poor thermal stability, low porosity, and insufficient electrolyte wettability [7] have often raised serious concerns about their fundamental functions to ensure the electrical isolation (cell safety) and ionic transport (cell performance) between electrodes. Among numerous approaches to overcome these limitations of polyolefin-based separators, the use of nonwovens comprising multi-fibrous layers has drawn considerable attention, as they offer excellent thermal resistance, high porosity, and cost competitiveness. However, conventional nonwovens face some challenges in providing well-tuned porous structure that can be directly applicable as a separator for lithium-ion batteries. More specifically, the excessively large pore size and nonuniform pore size

distribution of the nonwovens tend to inadequately prevent leakage current between electrodes, which results in an open circuit voltage (OCV) drop of cells [5–7]. Several attempts to resolve the aforementioned drawbacks of nonwovens have been reported, which include the coating of ceramic powders/binders to nonwovens [8–10], use of electrospinning-based nanofiber nonwovens [11,12], and impregnation of gel polymer electrolytes into nonwovens [13–15].

Meanwhile, two- or three-dimensionally close-packed arrangements of colloidal particles have been extensively investigated as ideal starting templates for the preparation of micro- and nanostructured periodic porous materials that could be used in various applications such as sensors, catalysts, and photonic crystal devices [16–20].

In the present study, by exploiting the intriguing concept of these colloidal particle arrays, we demonstrate a novel and facile approach to finely tune a porous structure of a nonwoven composite separator (hereinafter, referred to as an NC separator), which could be recommended as a promising alternative to conventional polyolefin separators. This strategy is based on the construction of silica (SiO_2) colloidal particle-assisted nanoporous structure in a poly(ethylene terephthalate) (PET) nonwoven substrate. Herein, the nanoparticle arrangement arising from evaporation-induced self-assembly of SiO_2 colloidal particles allows the evolution of the unusual nanoporous structure, i.e. well-

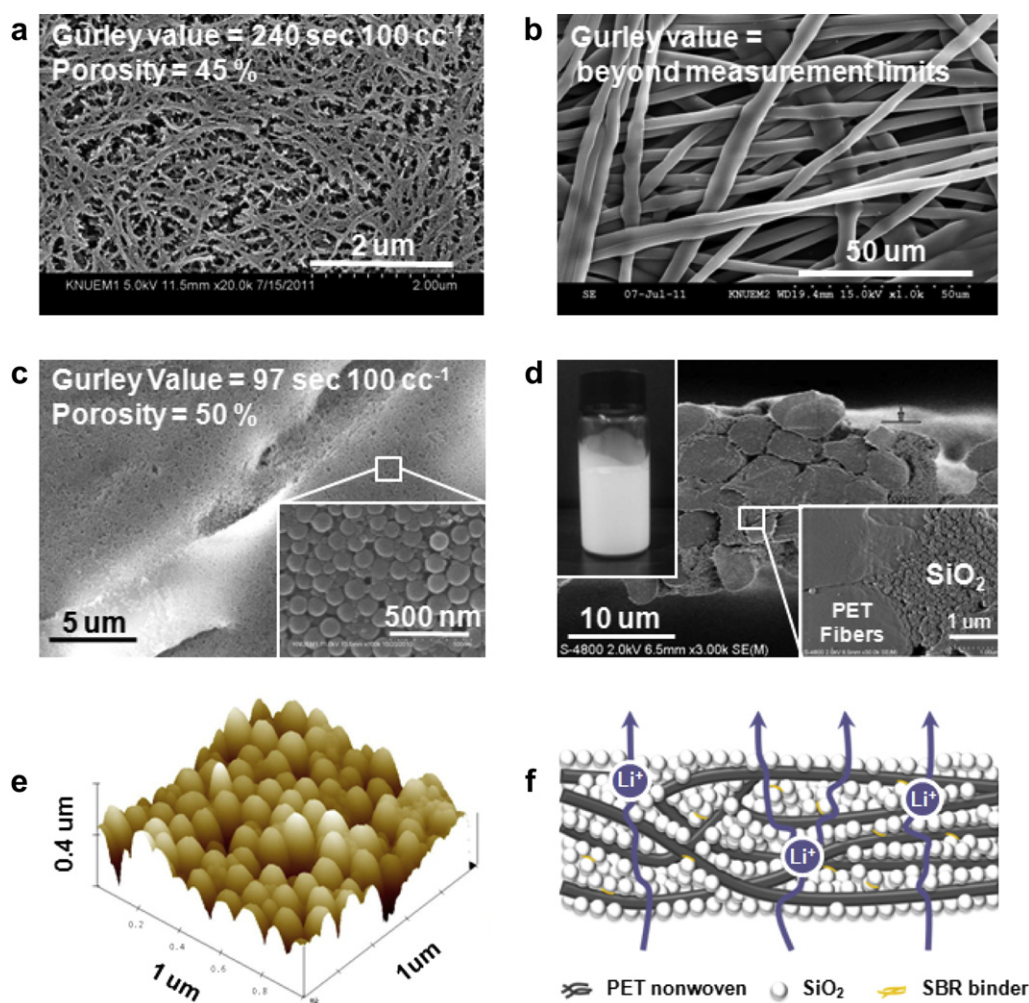


Fig. 1. FE-SEM photographs of: (a) PE separator (surface); (b) pristine PET nonwoven (surface); (c) NC separator (surface); (d) NC separator (cross-section, the inset is a photograph of the SiO_2 colloidal solution). (e) An AFM photograph of the NC separator. (f) A schematic representation illustrating the porous structure and conceptual ion transport of the NC separator.

connected interstitial voids formed between close-packed SiO₂ particles adhered by styrene-butadiene rubber (SBR) binders. The PET nonwoven serves as a mechanical support that contributes to preventing thermal shrinkage of the NC separator.

Performance superiorities of the NC separator, as compared to a commercialized PE separator, are evaluated in terms of porous structure, thermal shrinkage, electrolyte wettability, and ionic transport. Based on this characterization, advantageous effects of the NC separator on cell performance (specifically, OCV (Open Circuit Voltage) drop, discharge capacities, discharge C-rate capability, and cyclability) are also investigated.

2. Experimental

2.1. Fabrication of NC separator

A coating solution (inset in Fig. 1(d)) was prepared by mechanically mixing a SiO₂ colloidal solution (average particle size ~80 nm, Nissan) with an SBR emulsion (Synthomer) for 2 h. The solid content (= total amount of SiO₂ and SBR) in the coating solution was 18 wt% and the SiO₂/SBR composition ratio was fixed at 95/5 wt%/wt%. Herein, the influence of the SBR binder itself on the properties of the NC separator is assumed to be insignificant due to its very small content, in comparison to the SiO₂ colloidal particles. A PET nonwoven (average thickness = 17 μm, Mitsubishi) was chosen as a mechanical/thermal support. The PET nonwoven was soaked in the coating solution for 3 min by dip-coating. The evaporation-induced self-assembly of SiO₂ colloidal particles was realized between the PET fibers by slowly drying the coating solution-immersed PET nonwoven at room temperature, followed by vacuum drying at 60 °C for 4 h. The final thickness of the NC separator was approximately 18~20 μm. As a control sample, a commercialized PE separator (average thickness = 20 μm, Tonen) was chosen.

2.2. Characterization of membrane properties and electrochemical performance of NC separator

The morphologies of the separators were investigated using field emission scanning electron microscopy (Hitachi) and tapping mode-atomic force microscopy (Digital Instruments). The air permeability of the separators was examined with a Gurley densimeter (Gurley), where a low Gurley value (sec 100 cc⁻¹) indicates high air permeability [5–7]. The porosity of NC separators, Φ_p (%), was estimated using the following equation [10,21–23]:

$$\Phi_p(\%) = \{1 - [(W_c/P_c + W_N/P_N)/V_{NC}]\} \times 100$$

where W_c is the weight per square meter of the SiO₂/SBR coating layer (= 4.88 g), W_N is the weight per square meter of the PET nonwoven (= 10.04 g), ρ_c is the density of the SiO₂/SBR coating layer (= 2.08 g cc⁻¹), ρ_N is the density of the PET nonwoven (= 1.40 g cc⁻¹), and V_{NC} is the volume of the NC separator (= 1.9×10^{-5} m³). The pore size and pore size distribution of the separators were measured by a bubble-point test performed to the ASTM standard F316 using a porosimeter (PMI) [10,15]. For evaluation of electrochemical performance of the separators, a liquid electrolyte of 1 M LiPF₆ in ethylene carbonate (EC)/diethyl carbonate (DEC) = 1/1 v/v (Technosemi Chem) was used. The electrolyte uptake of the separators was determined by measuring the weight difference between the dry state and electrolyte-swollen state. A unit cell (2032 coin) was assembled by sandwiching a separator between a natural graphite anode and a LiCoO₂ cathode, and then activated by filling the liquid electrolyte. The charge/discharge capacities of the cells were examined using a cycle tester (PNE Solution). The discharge current

densities were varied from 0.2 to 2.0 C at a constant charge current density of 0.2 C under a voltage range of 3.0–4.2 V. The cells were cycled at different charge/discharge current densities of 0.5 C/0.5 C and 1.0 C/1.0 C, respectively. The AC impedance of the cells was measured using an impedance analyzer (Bio-Logic) over a frequency range of 10⁻²–10⁶ Hz.

3. Results and discussion

In contrast to a PE separator having large number of small-sized micropores (Fig. 1(a)), of which average diameter appears to be below 0.1 μm, the pristine PET nonwoven shows excessively large-sized pores that are arbitrarily distributed between the PET fibers (Fig. 1(b)). The morphological characterization of the NC separator (Fig. 1(c)–(e)) demonstrates that the close-packed nanoparticle arrangement driven by evaporation-induced self-assembly of SiO₂ colloidal particles allows for the evolution of a unique nanoporous structure, i.e. well-connected interstitial voids. The cross-sectional morphology (Fig. 1(d)) exhibits that the SiO₂ nanoparticles are compactly embedded between the PET fibers in the thickness direction. The AFM photograph (Fig. 1(e)) also confirms the development of a SiO₂ colloidal particle-assisted nanoporous structure in the NC separator.

The nanoporous structure of the NC separator is quantitatively evaluated by measuring its Gurley value. Compared to the PE separator (= 240 s 100 cc⁻¹), the NC separator presents a lower Gurley value (= 97 s 100 cc⁻¹). Meanwhile, the Gurley value of the pristine PET nonwoven was too low to be exactly determined, i.e. it was beyond the measurement limits of the Gurley densimeter, revealing that the pristine PET nonwoven has immoderately large-sized pores. A low Gurley value of a separator indicates high air permeability, i.e. a short tortuous path for air transport [5–7]. This difference in the Gurley value between the separators was confirmed by measuring their porosity. Fig. 1 also shows that the porosity of the NC separator is 50%, relative to that (= 45.0%) of the pristine PE separator. Thus, the

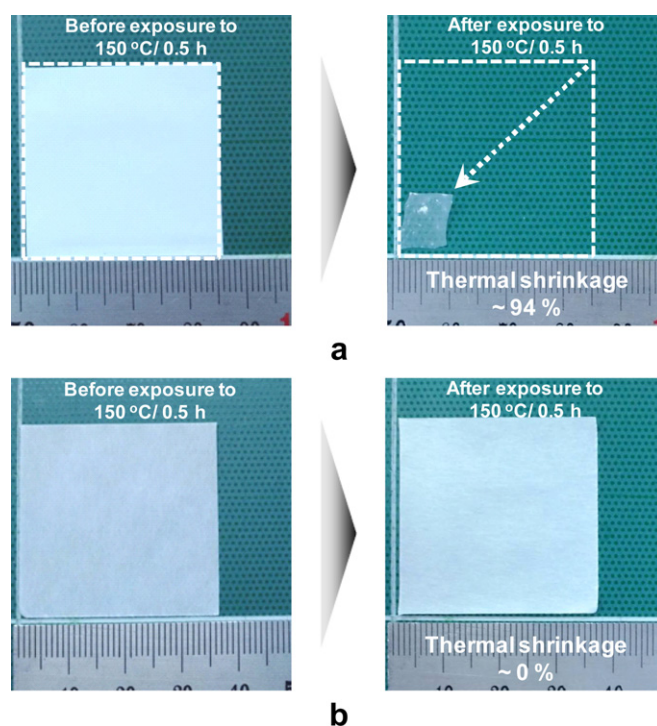


Fig. 2. Thermal shrinkage (after exposure to 150 °C for 0.5 h) of: (a) PE separator; (b) NC separator.

lower Gurley value and higher porosity of the NC separator, as compared to those of the PE separator, verify the successful development of the highly porous structure. This uncommon nanoporous structure is expected to critically influence the electrolyte wettability and ionic conductivity of the NC separator. A schematic representation illustrating the porous structure (i.e., well-connected nanosized interstitial voids) and conceptual ionic transport of the NC separator is provided in Fig. 1(f).

The thermal shrinkage of the NC separator was compared with that of the PE separator by measuring the (area-based) dimensional change after exposure to 150 °C for 0.5 h Fig. 2 exhibits the superior thermal stability of the NC separator (Fig. 2(b)), in comparison to the PE separator showing thermal shrinkage of ~94% (Fig. 2(a)). This substantially mitigated thermal shrinkage of the NC separator is attributed to the presence of the thermally stable PET nonwoven substrate [8–15]. The PET nonwoven substrate in the NC separator does not readily undergo thermal shrinkage, because it has a high melting temperature above 250 °C and is not subjected to stretching processes, which are generally employed to produce PE separators.

The intrinsically hydrophobic nature of polyolefin-based separators often leads to electrolyte wetting problems [5–7]. In particular, as the application range of lithium-ion batteries rapidly expands to new fields that generally require large-sized batteries, fast and uniform wetting of the liquid electrolyte over the entire separator poses a formidable challenge. Fig. 3(a) shows that the NC

separator is quickly wetted by the liquid electrolyte and also affords larger electrolyte uptake (~161% (NC separator) vs. ~117% (PE separator)). The electrolyte wettability is further examined by comparing the electrolyte immersion-height of the separators (Fig. 3(b)). The NC separator presents greater electrolyte immersion-height than the PE separator, which indicates facile capillary intrusion of the liquid electrolyte into the pores of the NC separator. This improvement in the electrolyte wettability of the NC separator is ascribed to its relatively polar (i.e., electrolyte-philic) constituents and the nanosized porous structure (i.e., highly-connected interstitial voids), both of which may facilitate capillary intrusion [24,25] of the liquid electrolyte into the electrolyte-philic pores.

The porous structure of separators is known to crucially affect the OCV behavior of cells [5–7,10,15]. An OCV drop reflects self-discharge of cells and possibly predicts the risk of internal short-circuits. Herein, the cells were charged to 4.2 V and their voltage drop was measured as a function of elapsed time. It is of note that there is little difference in the OCV profiles between the NC separator and PE separator (Fig. 4(a)). On the other hand, the cell assembled with the pristine PET nonwoven shows a sharp drop of OCV. This OCV behavior can be explained by considering the pore size and pore size distribution of the separators. Fig. 4(b) exhibits that, due to the presence of the close-packed SiO₂ colloidal particles, the NC separator offers not only small pore size (most of the pore diameters are below 0.1 μm) but also a narrow pore size distribution, both of which are comparable to those of the PE separator. By contrast, the pristine PET nonwoven presents much larger pore size (>5.0 μm) and broader pore size distribution. As

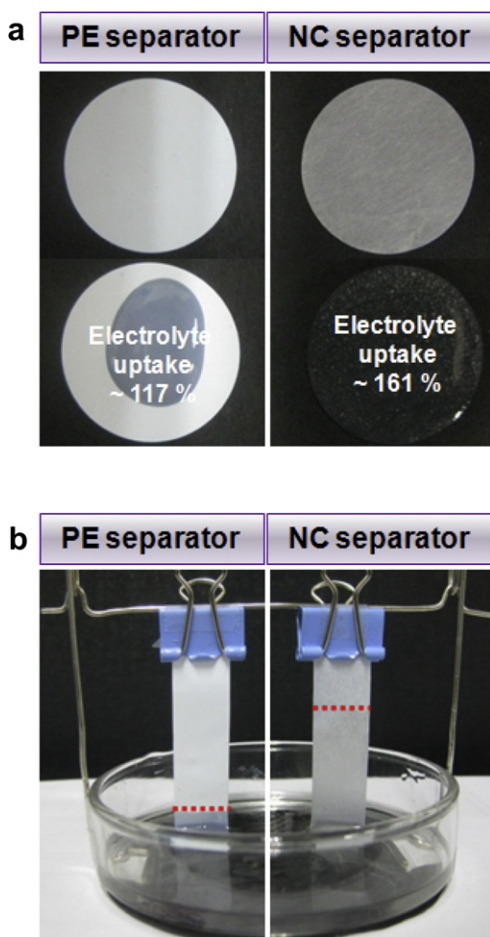


Fig. 3. (a) Photographs exhibiting liquid electrolyte (1 M LiPF₆ in EC/DEC = 1/1 v/v) wettability of PE separator and NC separator. (b) Liquid electrolyte immersion-height of PE separator and NC separator.

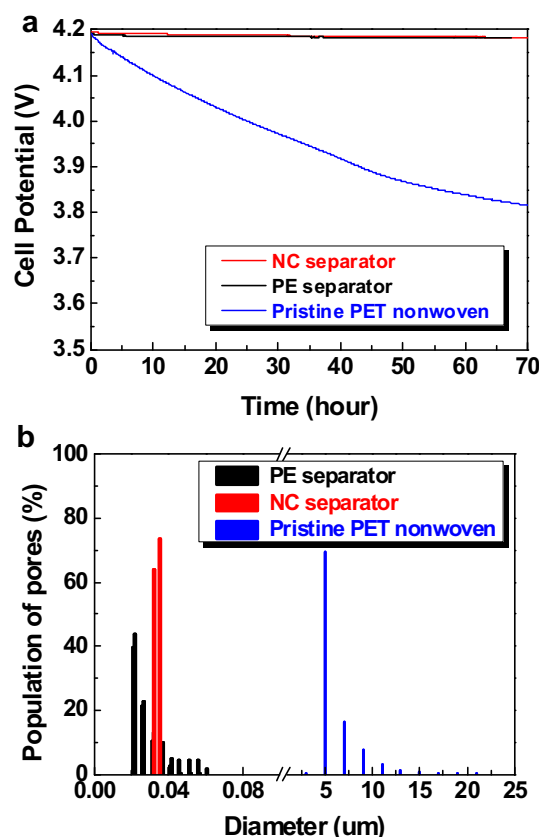


Fig. 4. (a) OCV profiles of cells assembled with different separators, wherein the cells are charged to 4.2 V at a constant charge current density of 0.5 C and their voltage drop is measured as a function of elapsed time. (b) Pore size distribution of PE separator, NC separator, and pristine PET nonwoven.

a result, it is believed that the porous structure of the NC separator is sufficiently tuned to suppress the self-discharge of the cells.

The cell performances of the NC separator at various charge/discharge conditions were investigated (Fig. 5). The voltage and discharge capacity of the cells gradually decrease with an increase of the discharge current density. No abnormal or unstable discharge profiles were observed in the NC separator. Under a voltage range of 3.0–4.2 V and given current densities, the discharge capacities of the NC separator (Fig. 5(a)) are higher than those of the PE separator (Fig. 5(b)). Interestingly, this difference in the discharge capacities between the separators becomes larger at higher discharge current densities where the influence of ionic transport on ohmic polarization is significant [8–13,24,25]. Fig. 5(c) summarizes the discharge capacities of the separators as a function of the discharge current density (i.e., discharge C-rate). Previous results (Figs. 1–3) revealed that the NC separator has a well-developed nanoporous structure and large electrolyte uptake. These advantages of the NC separator could provide high ionic

conductivity ($\sigma = 0.87 \text{ mS cm}^{-1}$ (NC separator) vs. 0.73 mS cm^{-1} (PE separator)), which is expected to improve the discharge C-rate capability.

The cycle performance (i.e., discharge capacities as a function of cycle number) of the NC separator was compared with that of the PE separator. The cells were cycled up to 100th cycles at different charge/discharge current densities of 0.5 C/0.5 C and 1.0 C/1.0 C. Fig. 6(a) shows that under a charge/discharge condition of 0.5 C/0.5 C, the NC separator presents higher discharge capacities than the PE separator. Notably, the difference in the discharge capacity between the separators becomes more pronounced at a higher current density ($= 1.0 \text{ C}/1.0 \text{ C}$), which boosts the influence of IR drop (Fig. 6(b)). This remarkably improved cycle performance of the NC separator may be attributed to its highly-developed nanoporous structure and strong affinity for liquid electrolyte, which could play viable roles in delivering more facile ion transport and better electrolyte retention [6,7,10,15] during cycling.

The improved cyclability of the NC separator can be further confirmed by analyzing the AC impedance spectra of cells after the 1st and 100th cycle. Cycle performance is known to be strongly affected by variation of cell impedance [26–29]. A possible equivalent circuit of general lithium-ion cells has been suggested in previous publications [27–32], which demonstrates that the semicircle of impedance spectra at the high frequency range represents the resistance of surface films on electrode materials and the semicircle observed at the medium-to-low frequency region can be ascribed to the charge transfer resistance between electrode materials and liquid electrolyte. Fig. 7 shows that after

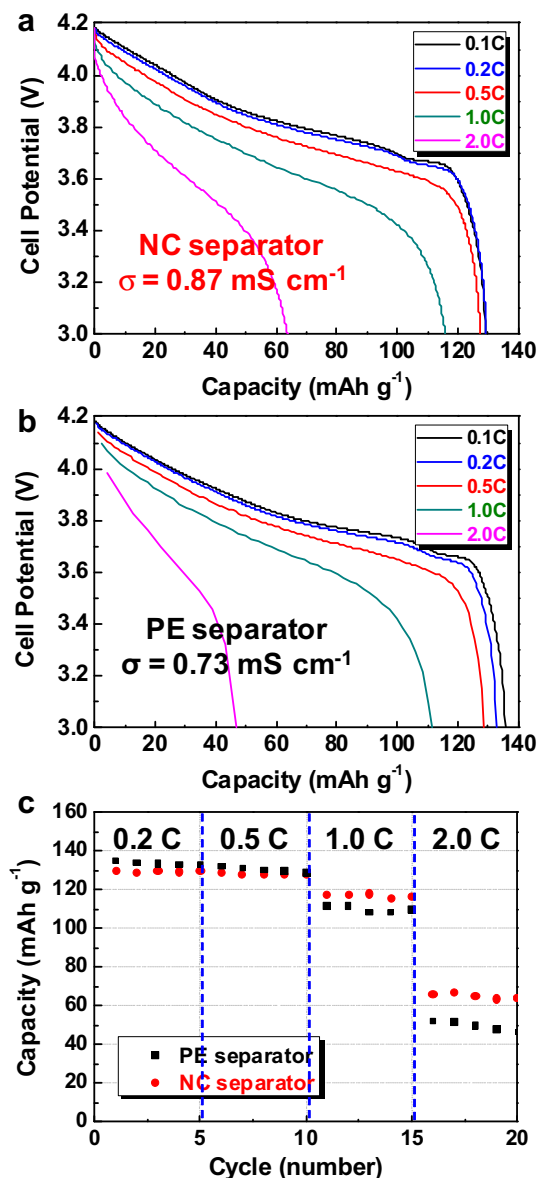


Fig. 5. Discharge profiles of cells assembled with: (a) NC separator; (b) PE separator. (c) Comparison of discharge C-rate capability between different separators.

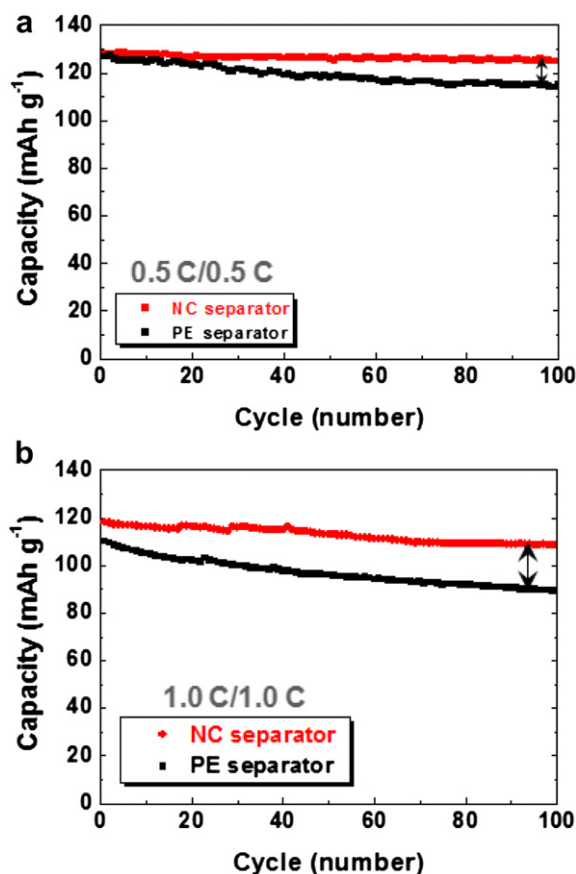


Fig. 6. Cycle performance of cells assembled with NC separator or PE separator at charge/discharge conditions (under a voltage range of 3.0–4.2 V) of: (a) 0.5 C/0.5 C; (b) 1.0 C/1.0 C.

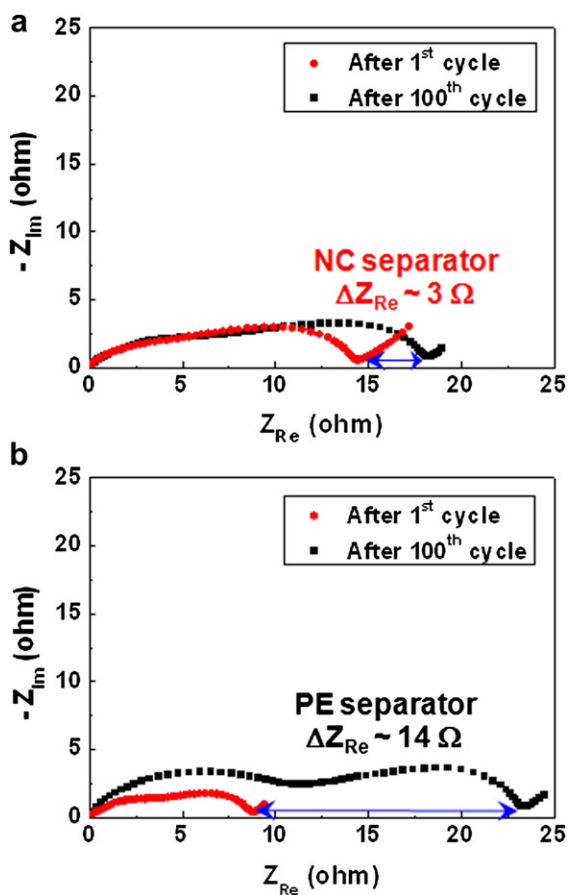


Fig. 7. Variation in AC impedance spectra of cells after 1st and 100th cycle (at a charge/discharge condition of 0.5 C/0.5 C): (a) NC separator; (b) PE separator.

the 100th cycle, the growth in the cell impedance ($\Delta Z_{Re} \sim 3 \Omega$) of the NC separator is retarded, as compared to that ($\Delta Z_{Re} \sim 14 \Omega$) of the PE separator. The suppressed growth of cell impedance reflects the stabilized interface between the NC separator and electrodes. This may be due to the benign contact of the liquid electrolyte-filled NC separator (more specifically, the SiO_2 coating layer featuring well-developed, electrolyte-philic interstitial voids) with the electrodes during cycling, which could in turn allow a more facile ion transport through the interface between the electrode materials and liquid electrolyte-filled NC separator. Previous studies [33,34] reported that the introduction of ceramic coating layers to separators was an effective way in retarding the growth of cell impedance, which in turn contributed to the better cycle performance.

4. Conclusion

In this study, the new NC separator, featuring SiO_2 colloidal particle-assisted nanoporous structural evolution, has been fabricated as a promising alternative to commercialized PE separators. The nanoparticle arrangement arising from the evaporation-induced self-assembly of SiO_2 colloidal particles in a PET nonwoven substrate allowed the development of the unusual nanoporous structure, i.e. well-connected interstitial voids formed between close-packed SiO_2 particles adhered by SBR binders. Due

to this structural novelty, the NC separator exhibited the low thermal shrinkage, highly porous structure (i.e., low Gurley value), excellent electrolyte wettability, facile ionic transport, and good compatibility with electrodes, in comparison to the PE separator. These advantageous characteristics enabled the NC separator to offer the significantly improved cell performance (particularly at high discharge current densities), which demonstrated its potential application to high-safety/high-rate lithium-ion batteries. A notable contribution of the present study is the provision of a facile route to fine-tune the porous structure of nonwoven-based separators by exploiting the anomalous architecture of close-packed SiO_2 colloidal particle arrays.

Acknowledgments

This work was supported by the National Research Foundation of Korea Grant funded by the Korean Government (MEST) (NRF-2009-C1AAA001-2009-0093307).

References

- [1] J. Hassoun, S. Panero, P. Reale, B. Scrosati, *Adv. Mater.* 21 (2009) 4807.
- [2] C. Liu, F. Li, L.P. Ma, H.M. Cheng, *Adv. Mater.* 22 (2010) E28.
- [3] J.B. Goodenough, Y. Kim, *Chem. Mater.* 22 (2010) 587.
- [4] G. Jeong, Y.U. Kim, H. Kim, Y.J. Kim, H.J. Sohn, *Energy Environ. Sci.* 4 (2011) 1986.
- [5] G. Venugopa, J. Moore, J. Howard, S. Pendalwar, *J. Power Sources* 77 (1999) 34.
- [6] P. Arora, Z. Zhang, *Chem. Rev.* 104 (2004) 4419.
- [7] S.S. Zhang, *J. Power Sources* 164 (2007) 351.
- [8] T.H. Cho, M. Tanaka, H. Ohnishi, Y. Kondo, M. Yoshikazu, T. Nakamura, T. Sakai, *J. Power Sources* 195 (2010) 4272.
- [9] S. Augustin, V. Hennige, G. Hoerpel, C. Hying, *Desalination* 146 (2002) 23.
- [10] E.S. Choi, S.Y. Lee, *J. Mater. Chem.* 21 (2011) 14747.
- [11] J.K. Kim, G. Cheruvally, X. Li, J.H. Ahn, K.W. Kim, H.J. Ahn, *J. Power Sources* 178 (2008) 815.
- [12] T.H. Cho, M. Tanaka, H. Onishi, Y. Kondo, T. Nakamura, H. Yamazaki, S. Tanase, T. Sakai, *J. Power Sources* 181 (2008) 155.
- [13] P. Kritzer, J.A. Cook, *J. Power Sources* 161 (2006) 1335.
- [14] Y.M. Lee, J.W. Kim, N.S. Choi, J.A. Lee, W.H. Seol, J.K. Park, *J. Power Sources* 139 (2005) 235.
- [15] H.S. Jeong, J.H. Kim, S.Y. Lee, *J. Mater. Chem.* 20 (2010) 9180.
- [16] C. Jiang, S. Markusya, Y. Pikus, V.V. Tsukuruk, *Nat. Mater.* 3 (2004) 721.
- [17] K.E. Mueggenburg, X.M. Lin, R.H. Godsmith, H.M. Jaeger, *Nat. Mater.* 6 (2007) 656.
- [18] S.H. Kim, S.J. Jeon, G.R. Yi, C.J. Heo, J.H. Choi, S.M. Yang, *Adv. Mater.* 20 (2008) 1649.
- [19] O. Schepelina, N. Poth, I. Zharov, *Adv. Func. Mater.* 20 (2010) 1962.
- [20] C. Li, L. Qi, *Adv. Mater.* 22 (2010) 1494.
- [21] T. Yamaguchi, F. Miyata, S. Nakao, *J. Membr. Sci.* 214 (2003) 283.
- [22] T. Yamaguchi, H. Kuroki, F. Miyata, *Electrochem. Commun.* 7 (2005) 730.
- [23] J.R. Lee, N.Y. Kim, M.S. Lee, S.Y. Lee, *J. Membr. Sci.* 367 (2011) 265.
- [24] J.H. Park, J.H. Cho, W. Park, D.J. Ryoo, S.J. Yoon, J.H. Kim, Y.U. Jeong, S.Y. Lee, *J. Power Sources* 195 (2010) 8306.
- [25] J.H. Park, W. Park, J.H. Kim, D.J. Ryoo, H.S. Kim, Y.U. Jeong, D.W. Kim, S.Y. Lee, *J. Power Sources* 196 (2011) 7035.
- [26] Y.K. Sun, J.M. Han, S.T. Myung, S.W. Lee, K. Amine, *Electrochem. Comm.* 8 (2006) 821.
- [27] Y.K. Sun, S.W. Cho, S.T. Myung, K. Amine, J. Prakash, *Electrochim. Acta* 53 (2007) 1013.
- [28] W. Chang, J.W. Choi, J.C. Im, J.K. Lee, *J. Power Sources* 195 (2010) 320.
- [29] J.H. Park, J.S. Kim, E.G. Shim, K.W. Park, Y.T. Hong, Y.S. Lee, S.Y. Lee, *Electrochem. Comm.* 12 (2010) 1099.
- [30] S.K. Hu, G.H. Cheng, M.Y. Cheng, B.J. Hwang, R. Santhanam, *J. Power Sources* 188 (2009) 564.
- [31] B.J. Hwang, C.Y. Chen, M.Y. Cheng, R. Santhanam, K. Ragavendran, *J. Power Sources* 195 (2010) 4255.
- [32] K.S. Lee, Y.K. Sun, J. Noh, K.S. Song, D.W. Kim, *Electrochem. Comm.* 11 (2009) 1900.
- [33] Z. Li, G. Su, X. Wang, D. Gao, *Solid State Ionics* 176 (2005) 1903.
- [34] H.S. Jeong, S.Y. Lee, *J. Power Sources* 196 (2011) 6716.